8. ENGINEERING MECHANICS AND MATERIALS

G. Mervin Ault

A portion of the emerging technology in engineering mechanics and materials may be of interest to the power industry. Some aspects of NASA work in these areas has been described in other papers of this conference. The subjects to be reviewed herein are

(1) Engineering mechanics
   (a) Materials in long-time service: prediction of long-time properties; metallurgical embrittlement
   (b) Thermal fatigue and low-cycle fatigue
   (c) Brittle fracture of metals

(2) Materials
   (a) Materials strengthened by dispersed inert particles
   (b) Composite materials from fibers

PREDICTION OF LONG-TIME PROPERTIES

When materials are used at high temperatures, a common design criterion is "stress to rupture" (fig. 8-1). At elevated temperatures, when a load is applied to a metal specimen, the specimen may not fail immediately, but with sustained application of that load the specimen slowly elongates or "creeps" until finally it does fracture. Thus, for every stress at each temperature there is a finite time to fracture. To determine each data point used to define these curves, a specimen is loaded into a machine and left in the machine at temperature and under load until it fractures. If design data were needed for times of 100 000 hours ($11\frac{1}{2}$ yr), many machines would be in use for a long time.

In recent years, interest has increased in long-time properties. In aircraft jet engines operating lives as long as 15 000 to 30 000 hours (2 to 4 yr) are desired, and in space power systems operating lives of at least 5 years. For earth-bound power systems the need is for much longer operating lives of 20 to 40 years. Thus, there exists a common interest in drastically reducing the testing time to obtain design data. For example, if a device that will last 20 years is needed, a delay of

20 years to obtain design data before starting to build hardware is obviously unacceptable. It is thus desirable to have proven methods for extrapolating test data obtained in short times out to long times.

Several methods have been developed for this purpose. These methods generally depend on the substitution of temperature for time, as indicated on figure 8-2. (This figure is the same as fig. 8-1 except that the dashed lines have been added.) Suppose there is interest in the stress-rupture time for 40 000 psi and 1200° F. The figure shows that the rupture time is 10 000 hours. If the test could be made at the same stress, but at 100° F higher temperature, the test time would be cut by a factor of 10 to only 1000 hours. This transposing of temperature for time is possible if the mathematical relations among such data can be determined for a material. Methods for determining such relations have been developed, and they are generally known as "correlating methods," or "time-temperature parameters." Good success has been achieved with a parameter method developed at this Center, known as the Manson-Haferd parameter (ref. 1).

The Manson-Haferd parameter has been evaluated for a very large number of materials. An example of its use is illustrated in figure 8-3 for 17-22AS steel (ref. 2). In the upper right corner is shown the equation that describes the behavior of this material in terms of temperature T and time t. The constants are derived for each material by a prescribed systematic procedure (ref. 3) that uses a minimum of data. The correlating lines for the data are shown as solid lines, and the actual data as circular symbols. A good fit is indicated.

Once the parameter is determined, some interpolations and extrapolations of data are possible (i.e., if the designer wishes to know a reasonable approximation of the properties at another temperature, the parameter provides a rational basis for this interpolation as suggested in fig. 8-3 by the dashed line at 940° F).

Inadvertently, an opportunity arose to check a rather large extrapolation with this material. A specimen of 17-22AS steel was set up in the machine at 940° F with a stress intended to cause failure in much less than 1000 hours. The specimen was incorrectly loaded, however, and the stress was actually only one-half of that planned. After it had been in the machine for an appreciable length of time and had run well beyond the expected life, the mistake was discovered - it was found that the actual stress was only 40 000 psi. The specimen finally failed at 24 000 hours and was a good fit (fig. 8-3) to the line predicted by the parameter.

Although the parameter methods have been evaluated for a large number of materials in the 100- to 1000-hour time range, it is not often that data are available to much greater times, as was the case for the 17-22AS steel. An opportunity (ref. 4) to check the parameter methods to even longer times was provided through tests that were being run in Germany to evaluate several steels for steam turbine appli-

cations. The German investigators were running tests for 10 or 11 years, or nearly 100 000 hours. An example from the program is shown in figure 8-4. The NASA obtained material from these scientists and ran specimens over the time spectrum indicated on the figure (i.e., from 10 to about 3000 hr). From these relatively short-time tests the constants in the parameter were determined, and the predictions were made (solid curves in fig. 8-4). (The parameter here is a more general parameter than shown in the previous figure.) The data points are those obtained by the German investigators with their specimens in their test facilities. The general fit is quite good (e.g., the triangle on the right of the curve for 1202° F is at a time close to 100 000 hr, and it agrees quite well with the predicted line).

In general the so-called "time-temperature parameters" have proved very useful in minimizing testing and are now widely used.

A problem frequently encountered in long-time exposure of materials is metallurgical instability. An example is shown in figure 8-5 which illustrates the formation of a brittle phase known as "sigma phase" in the alloy IN-100, which is a commonly used bucket alloy. The two sets of stress-rupture data in the figure are for the alloy with only very slight differences in composition. The structure of the two compositions as revealed in the metallurgical microscope is shown in the two photographs, which differ in that the left one shows fine lines. These lines are the brittle sigma phase. As can be seen from the data plots, the one with sigma is weaker, and also there is a sharp break in the strength curve after a period of time. This is the time when sigma forms in the alloy. This formation of sigma in the alloy and the simultaneous break in the curve indicate instability. Unforeseen instabilities in alloys of this particular type would generally raise questions regarding extrapolations of data using time-temperature parameters. Currently, the problem of extrapolation of properties for such unstable materials is being examined.

It is even more important to learn how to design alloys so that such time-dependent instabilities do not occur. In addition to lowering high-temperature properties, the sigma phase may make the alloy brittle at room temperature.

Several General Electric Co. investigators (ref. 5) have developed a prediction method for avoiding sigma phase. The method involves using the alloy composition to calculate the electron vacancy concentration N_v of the residual matrix after other phases, such as γ' and the carbides, have precipitated. The electron vacancy concentration indicates the tendency for certain elements in the alloy to combine and form the undesirable phase, sigma. It has been found that as N_v goes above 2.48 (fig. 8-6) there is an increasing tendency to form sigma and as it goes below that value there is a lesser tendency. Many stainless steels are well into the sigma range and form the phase. The important high-temperature superalloys of

nickel base vary in their tendency, as indicated in the figure. Some important ones are on the border line, and slight changes in composition or processing can tip the balance. The superalloys of cobalt base do not form sigma, but they can form other embrittling phases. Studies of the embrittlement of HS-25 alloy are presented in references 6 to 8. This NASA laboratory is conducting studies to better define the parameters for avoidance of sigma phase in a sensitive nickel-base alloy (fig. 8-5), and to understand the embrittlement of cobalt alloys. Several other organizations are working on the development of high-temperature alloys for the power industry that are of a cost and strength more comparable to the stainless steels but entirely free of the embrittling sigma phase. Good progress has been reported.

THERMAL FATIGUE AND LOW-CYCLE FATIGUE (LCF)

A failure mechanism that is too often encountered in materials at high temperatures is thermal fatigue. Figure 8-7 shows an example of such failure for a steam power system component. The NASA has had considerable experience with such failures in gas turbines. Examples of thermal fatigue failures in turbine disks and buckets are shown in figure 8-8. Failures of this type may occur whenever materials operate with temperature gradients in a cyclic mode. The temperature gradients may occur either under steady-state operation or during starting and stopping. Basically the problem is that metals expand or contract when heated or cooled. If they are not permitted to expand or contract freely, something must give, and, thus, the metals flow plastically. The mechanism of thermal fatigue failure is illustrated in figure 8-9.

The turbine blade in figure 8-8 has a thin leading edge with a thicker adjacent section. Schematically, it is similar to the illustration in figure 8-9, where a thin section is attached rigidly to a thick section. If hot gases are passed across the structure, the thin section heats more rapidly than the thick section and tries to expand to a new length, as indicated by the dotted areas. Because it is rigidly attached to the thick section, however, it cannot expand as it desires. The free expansion is constrained by compressive forces from the attached heavy section. Because it cannot expand, something must give - the thin section flows plastically, as shown schematically in the right view of figure 8-9. This flow occurred during heating. If the structure is now cooled, the process is repeated, but in reverse; the thin section is pulled in tension and flows in tension. Upon repeated temperature cycles, the material goes through repeated compression and tension strain cycles until finally it cracks.

An objective of NASA research is to develop methods to predict, for any opera-

ting component, the cycles to failure in thermal fatigue. To achieve this the ability to compute certain factors is essential. From the environment the temperature gradients that will occur in the part and then the actual local strains must be computed. The strain calculation would not be too difficult if only elastic conditions were involved, but complex plastic strains must be included as well. If the plastic strains can be calculated, the relation between the cyclic strains and cycles to failure must be determined for any material.

Some years ago it was found, from simple laboratory tests, that there was a relation between the amount of plastic strain per cycle and the cycles to failure. This is the Manson-Coffin relation for plastic fatigue (refs. 9 and 10), which is shown in figure 8-10.

In recent years, Lewis has conducted more detailed studies to predict thermal fatigue failures of materials, starting with the relatively simple case of mechanical fatigue at constant temperature. Shown in figure 8-11 is a typical mechanical fatigue curve where cyclic stress is plotted against cycles to failure. These curves usually become horizontal beyond 10^6 to 10^8 cycles, and this is called the fatigue limit. With cyclic stresses below this line, the material should run forever. In mechanical fatigue attention has been directed toward factors affecting this fatigue limit. In thermal fatigue there is more interest in cycles to failure of much less than 10^5 - frequency 5000 and sometimes as few as 10 to 100. This is the range where for a particular cyclic stress there is a finite number of cycles to failure, which is the low-cycle fatigue (LCF) range. Thus, considerable attention is directed toward this portion of the fatigue curve. In thermal fatigue cyclic strains due to restraint of free thermal expansion are encountered, and thus laboratory tests are run with controlled cyclic strain rather than cyclic stress. (The shape of the curve is the same.)

In studying this region of the curve it has been found at Lewis that instead of having to run many fatigue specimens to define the LCF properties of a material, a reasonable approximation of the LCF properties can be achieved from a simple tensile test (ref. 11). A tensile test is run by taking a specimen and pulling it until it fractures. From the stress-strain curve (fig. 8-12) of the short-time tensile test three values are measured, the slope of the stress-strain curve (the modulus of elasticity E), the ultimate strength S_u, and a measure of the total strain of the material D (actually the reduction of area of the specimen cross section is used). By an empirical method developed at this laboratory and known as the method of universal slopes, the LCF curve can then be drawn (fig. 8-13). From the strength of the material and the modulus of elasticity, the elastic relation is drawn. From the ductility, that is, the plastic flow capability of the material, the plastic relation is drawn. The LCF strength curve is the sum of those lines. Of interest is that for

few cycles to failure, the LCF strength is controlled by the plastic properties of the material and for many cycles to failure the LCF strength is controlled by the elastic and strength properties of the material. For good LCF strength, materials are required to have good plastic flow capability and good strength.

The value of the universal slopes method for estimation of LCF from short-time tensile tests at room temperature is illustrated in figure 8-14 for four materials. The method has been tested on more than 60 materials with consistently good results. If precise LCF data are needed for design, the method of universal slopes can be used to provide guidance for planning the test program and to minimize the required testing.

Recently, efforts have been made to extend this prediction method from near room temperature to high temperatures within the creep range (ref. 12). At these high temperatures, the mechanism of material behavior is much different. The fact that the materials are in their creep range means that even under a constant load they will continue to flow plastically. Creep can cause the mechanism of cracking to change, too. As a result it has been necessary to modify the method of universal slopes for application at high temperatures in the creep range by the 10 percent rule. By a method described in reference 12 the 10 percent rule permits estimation of the average life in LCF at these high temperatures within the creep range (fig. 8-15). It has been found that the data show quite wide scatter about this predicted average at high temperatures, however. If a designer wished to draw a conservative lifeline to ensure, for example, only 1 percent failure probability, he would need to draw a new line (dashed line in fig. 8-15) about 1 order of magnitude of failure cycles below the derived line. This conclusion is based on the preliminary examination of 40 sets of high-temperature LCF data from many investigators.

A part of current NASA research in high-temperature LCF is directed toward understanding additional factors that must be taken into account to improve the estimation. For example, one factor is almost obvious. Creep occurs at high temperature. Thus, in addition to the magnitude of the cyclic strain, at high temperatures how fast that strain is applied (i.e., the strain rate) is of concern. An example (ref. 13) is shown in figure 8-16. The data points of figure 8-16 show the actual low-cycle-fatigue data. The lower curve is the estimated LCF from short-time tensile tests that were run at conventional strain rates, but those rates were far different from the strain rate of the LCF tests. When the strain rate of the short-time tensile test was rerun at strain rates that matched those of the LCF test, a much better estimation was obtained.

The material discussed herein has emphasized the studies undertaken at Lewis to estimate and understand LCF at constant temperatures. Thermal fatigue and

LCF are essentially the same except that in thermal fatigue the strain cycle occurs over a range of temperatures and thus the material properties change as the temperature changes. The process is, therefore, more complex than that for constant-temperature LCF. Significant knowledge has been gained on the more complex situation, and considerable effort has been directed against the total problem of prediction of cycles to failure of a component in a complex environment.

BRITTLE FRACTURE OF METALS

Another evolving technology of importance in the application of metals is fracture mechanics. It has been particularly important for NASA to contribute to this development because of the need to use very high-strength alloys of steel, aluminum, and titanium. Figure 8-17 shows the test firing of the world's largest solid rocket, commonly called the 260-inch rocket. This has been an outstandingly successful test program. Three test firings have been conducted, and in one firing a thrust of 5.6 million pounds was achieved from this single engine. The size of the case containing the propellant is indicated in figure 8-18. The diameter is 260 inches or about 22 feet, and the overall length is $62\frac{1}{2}$ feet. To save weight in such a large engine, high-strength steels with strengths perhaps five times those used in steam boilers and reactor pressure vessels must be used. In this particular case the metal is stressed to about 135 000 psi. The use of these high-strength steels operating at high-stress levels permits a wall thickness of about 0.6 inch in this application, and thus considerable weight is saved. (Wall thicknesses in boilers and reactor pressure vessels may be as great as 6 to 20 in.)

Unfortunately, there are occasions where large hardware fails. A failure of a large steam turbine is shown in figure 8-19. In the development phase of another version of the large solid rocket failure occurred, as shown in figure 8-20. This failure occurred during a water pressure test of a particular fabrication method for this propellant case. An important feature of this failure should be noted. When metals fail, they usually stretch and bend while tearing, and finally break into only two pieces. This propellant case looks very brittle - it has shattered in a manner more characteristic of an eggshell than a metal.

After some elaborate detective work, the origin of the failure was found in the area indicated by the arrows in figure 8-20. Figure 8-21 is an enlarged photograph of a small part of the tank wall at this point. The metal was 0.7 inch thick. In the center of the photograph is a small area that was a crack in the original hardware. This crack was only 1/8 inch in the vertical or thickness dimension and about $1\frac{1}{2}$ inches long. Actually, this is only a very small crack in a very large tank, and

the crack removed only 0.01 percent of the load-carrying area of the tank material. One thus might think it would be of little importance. In reality, although the total load-carrying area was reduced by only 0.01 percent, the effect of this crack was to cause the tank material to fail at only one-half of its strength as conventionally measured in the laboratory.

The phrase "strength as conventionally measured" is important because this introduces the concepts of fracture mechanics. Interest in fracture mechanics is based on the concept that when metals are fabricated into hardware or structures, it is axiomatic that they do contain flaws or will develop them within their service lifetime, and these flaws or cracks can drastically change metal behavior. As shown for this large rocket case, a relatively small crack cut the conventional strength in half and led to a catastrophic brittle-type failure.

This behavior is illustrated in figure 8-22. Shown schematically are two specimens, each with a crack, being loaded in tension. The specimen on the left represents a ductile metal, and the one on the right a brittle metal. Consider the ductile metal first. As the load is increased on the specimen, the crack moves across the specimen, and the metal stretches and tears. Just ahead of the crack tip, because of the stress concentration effect of the crack, a plastic zone develops where the metal is stretching and yielding. In the ductile metal this plastic zone is large, but in a brittle metal that has little capability to flow plastically, only a very small plastic zone develops. As the load is increased on the ductile metal and the crack moves through the metal, a large amount of stretching and tearing occurs, and a large amount of energy is consumed. In the brittle metal, on the other hand, very little energy is consumed in propagating the crack. Thus, in the ductile metal a high load to failure and slow crack propagation result; but in the brittle metal the failure load is low, and once the crack starts to move it may never stop. Catastrophic failure may result. The large rocket case was a typical example. Another way to understand this is to consider the stress state at the front of a crack, plotted in the lower portion of figure 8-22. In an ideal brittle material no plastic flow can occur, and as the tip of a sharp crack is approached the elastic stress rises to a very high value. In metals, plastic flow can occur, and the stress is reduced at the crack tip. Thus, "ductile" metals are less sensitive to cracks than "brittle" metals.

Not only is crack sensitivity a function of the material, but part geometry also has an effect, as illustrated in figure 8-23. Below the ductile metal another sketch of the same metal is shown, but in this case the specimen is much thicker. Now, in thicker cross section, as the metal is loaded, the metal surrounding the crack creates a triaxial stress state that inhibits the plastic flow within the specimen. This drastically reduces the plastic zone size or in other words raises the stress

concentration. (The difference in plastic zone size occurs only within the metal specimen, not on the surface. They are shown as different on the surface for convenience in illustration.) Now a "brittle condition" exists and the crack propagates easily. For a high-strength metal conventionally described as ductile there can be either "ductile behavior" or "brittle behavior," depending on part thickness, crack size, and geometry.

The discipline called fracture mechanics is developing methods whereby the strength of structures containing flaws can be related to measureable quantities of materials. (See refs. 14 and 15 for a general discussion.) For an important stress condition called plane strain which is characteristic of cracks in thick parts, test procedures have now been developed whereby a new material property of fracture toughness K_{Ic} can be measured. The new test method has been accepted as a standard by the American Society for Testing and Materials (ref. 15); NASA researchers have been major contributors in the development of this new material property measurement.

If conditions of plane strain are not met in the hardware, it is necessary to run simulated service tests wherein the conditions of the hardware are simulated in the laboratory, but with artificially produced cracks.

The importance of considering the existence of cracks in real hardware is illustrated in figures 8-24 and 8-25, which are based on an example developed during the selection of materials for a particular application.

Figure 8-24 shows the conventional approach to material selection. Here the operating stress was to be 150 000 psi. Material B was a candidate. Its yield strength was 200 000 psi; dividing the yield strength by the operating strength gave a safety factor of 1.3. Material A, however, had a yield strength of 285 000 psi, resulting in a safety factor of 1.9. Material A was the obvious choice.

But what if the hardware contains a small crack? Figure 8-25 shows the measured fracture strength as a function of crack size. Material A is very sensitive to cracks, and with cracks of only 0.050 inch or larger the material would fail at or below the desired operating stress. Material B, on the other hand, would tolerate cracks of at least three or four times the size tolerated by material A. If there were absolute certainty that the structure would be crack free or that the inspection method could positively identify every crack greater than 0.050 inch, material A would be a possible choice. This small crack size, however, is almost impossible to detect in large hardware. Also cracks may develop in service. Thus, the preferred material would almost certainly be material B. It is the better material at any crack size greater than 0.030 inch.

Again, the important concept is that most hardware will almost certainly contain small cracks when produced or develop such flaws during its service lifetime.

This should be considered in the evaluation and selection of materials. The evolving technology of fracture mechanics is providing the tools to handle this problem for the application of high-strength metals. (A portion of the Lewis Research Center work in this general area is presented in refs. 17 to 24.)

METALS STRENGTHENED BY DISPERSED INERT PARTICLES

Let us now consider dispersion-strengthened metals. The particular advantage of this method of strengthening is that, in concept, it provides a method for extending the use temperature of any particular metal (e.g., aluminum, nickel, or copper (ref. 25)).

The reason for dispersion strengthening can be understood from the following example of nickel-base alloys with which NASA has worked for many years. Figure 8-26 shows the microstructure of a high-strength nickel-base alloy as seen at an original magnification of ×750. The small particles shown tend to key the structure - to make it resist flowing or deforming under load and thus to make it strong. For highest strengths, it is important that these particles be very small and very close together. Generally, the closer the particles are to each other, the greater the strength. Particles about 1/2-millionth inch in diameter and 10-millionths inch apart are desired. The metallurgist can alter this structure by heat treatment. At very high temperatures, the particles will dissolve into the solid matrix, and at lower temperatures the particles will reprecipitate or reform. Unfortunately, as an effort is made to use the alloys at higher and higher temperatures, the temperature at which the alloy is to be used is the temperature at which the particles dissolve into the matrix, and thus the strength is lost.

To raise the use temperature of alloys, metallurgists are developing new materials called "dispersion-strengthened" metals. The concept is to distribute small particles that will strengthen, but not dissolve into, the metal. This is best accomplished by the methods of powder metallurgy. Figure 8-27 shows the structure of such a material that has been produced at Lewis (ref. 26). This material was made by dispersing 4 volume percent of ultrafine particles of thorium dioxide (ThO_2) into pure nickel. The structure looks so different from the microstructures in figure 8-26 because this structure has been magnified to about ×11 000 (using the electron microscope) to show the ultrafine particles of ThO_2 (the dots in the structure). These ceramic particles will not redissolve in the metal even at the melting point of nickel (2650° F). Thus, they continue to serve their strengthening function at temperatures approaching the melting point of nickel.

Available commercial materials made in this way are aluminum oxide (Al_2O_3)

distributed in aluminum, thorium oxide in nickel, and beryllium oxide (BeO) in copper. The strength of the dispersion-strengthened nickel is shown in figure 8-28, which is a plot of stress for rupture in 1000 hours against temperature in ^{o}F. Shown by the dashed curve is the strength of a typical conventional superalloy of the type discussed previously. The solid curve represents dispersion-strengthened nickel (ref. 27). Most impressive is the flat slope of the strength curve for the dispersion-strengthened nickel; it does not lose strength rapidly as temperature is increased. Although the conventional alloys are stronger at low temperatures, they rapidly lose strength as temperature is increased, particularly in the range of 0.6 to 0.7 of the melting point, in part because the particles that are largely responsible for strengthening are dissolving into the metal. The thorium oxide particle in the dispersion-strengthened nickel is stable, and the strength is retained.

Another advantage of dispersion-strengthened metals is the opportunity to create materials with physical properties that are not possible in conventional alloys. Alloying severely reduces thermal conductivity and electrical conductivity. For example, just 2 percent of aluminum added to copper reduces the thermal conductivity of copper by 75 percent. This fact can be shown also for the nickel-base materials just discussed. Figure 8-29 shows the thermal conductivity of nickel and the conductivity of a high-strength nickel alloy. The alloy has only 10 percent of the conductivity of pure nickel. The previously described dispersion-strengthened nickel, strengthened by the addition of 2 volume percent of discrete particles of thorium oxide, has 90 percent of the conductivity of nickel. This result is expected because much of the material is still the pure metal, not an alloy, and the only interferences to conduction in this pure metal are the isolated discrete particles of ThO_2. But there is a free path of pure metal all around these particles, which make up only 2 to 4 volume percent of the structure.

Examples of dispersion-strengthened conductors are BeO particles dispersed in copper and Al_2O_3 particles dispersed in copper. Data for BeO in copper (ref. 28) are shown in figure 8-30. The strength of the dispersion-strengthened copper compared with that of cold-worked pure copper (upper part of figure) shows that the dispersion-strengthened material holds its strength to high temperature and has a clear advantage.

A plot of the resistivity of these materials (lower part of figure) shows, as expected, that the resistivity of the dispersion-strengthened copper is only slightly higher than that of pure copper.

Another case where dispersion strengthening is being investigated to develop high-temperature materials of unique properties is for magnetic materials. If magnetic metal alloys are sought for use at high temperatures, the first objective is to achieve maximum Curie temperature. Next, alloying additions are considered that

will strengthen this good magnetic material. The NASA has developed a new cobalt-base alloy by conventional strengthening methods that look very attractive for this purpose (ref. 29). However, as the metallurgist seeks alloying additions to improve the strength of such alloys, he finds that the additions that improve strength unfortunately degrade magnetic properties. Thus, he again turns to the methods of powder metallurgy and dispersion strengthening to achieve an increase in use temperature with little degradation in magnetic properties. Such studies are being conducted under NASA contract (e.g., Westinghouse contract NAS 3-6465), and some materials of interest have been identified.

FIBER-REINFORCED MATERIALS

Whiskers (fig. 8-31) are nearly perfect single crystals of materials that have strengths of about 3 000 000 psi, approaching the theoretical strength of materials, whereas the materials in use today have strengths of only 5 percent of theoretical. Unfortunately, these near theoretical strengths are available only from these tiny, fragile whiskers, but other fiber materials in polycrystalline form are available in greater lengths and are less fragile. Typical strengths are shown in figure 8-32.

The whiskers of graphite and Al_2O_3 have strengths of about 3 000 000 psi (top of the figure). On the lowest portion of the figure are shown the useful strengths (yield strengths) of typical conventional bar materials. The most familiar of the polycrystal fibers is "E" glass. This fiber is used in most industrial applications of composites, such as fishing poles and boats. Even stronger fibers are being developed, for example, silicon dioxide (SiO_2) and a new glass fiber, "S" glass. These fibers have 2 to 4 times the strength of high-strength steels. Also shown are the strengths of two metal wires, steel rocket wire and tungsten. The strengths of boron and graphite are also included. There are, of course, many weaker fibers that have not been plotted.

For aerospace applications lightweight materials are of particular interest. Thus, if material density were factored in, the heavier metal wires of steel and tungsten would be lower in relative standing and the others, because of their low weight, would have even greater advantage. A great deal is heard about boron and graphite fibers, but this comparison suggests that at their present state of development, strength is not their greatest asset. These two materials are of interest because of their exceptionally high modulus of elasticity which is of prime importance in many structures, particularly for aerospace use, where stiffness and light weight are the prime design criteria.

To utilize the strengths of fibers they must be assembled into a composite with

either a metal or plastic matrix. Figure 8-33 shows a typical composite specimen made by assembling tungsten wires into a matrix of copper. The circles are the tungsten wires of 0.005 inch diameter, and the area between is copper. Fishing poles are often made by binding glass fibers together with a matrix of plastic. As a general rule in composites, the more fiber that is packed into the composite, the higher the strength.

Because good bonding is obtained with W-Cu and no damaging reactions occur between the two, NASA has used this combination as a model system for fundamental research into micromechanics of composites, and many publications are available to describe the work in this area (ref. 30).

As in the case of dispersion-strengthened metals, fiber-reinforced metals offer an opportunity to find new materials that will have a higher use temperature than conventional alloys. In an attempt to find better high-temperature materials for jet engine turbine buckets, new materials have recently been made by embedding tungsten wires in a superalloy matrix. Methods have been found for assembling these tungsten wire - superalloy composites such that in laboratory tests at 2000° F specimens have three times the 100-hour rupture strength of conventional nickel-base alloys used today. Although they are very heavy materials, even on a stress-density basis these composites have a significant strength advantage over conventional alloys (ref. 31).

With fiber composites as with dispersion-strengthened metals, there is an opportunity to tailormake materials with the specific properties needed. This applies particularly to physical properties, such as conductivity or resistivity. For example, in the W-Cu model system, the copper in the matrix provides high conductivity (or low resistivity), and the tungsten wires provide strength. The composite should have high strength and low resistivity, and a wide range of these properties is possible depending on the volume percent of tungsten wires in the composite.

Figure 8-34 shows some interesting data for this system (ref. 32). The parameter plotted is the ratio of strength to resistivity, and high values may be sought for some conductor applications. In the center portion of the figure is shown the range of values for W-Cu composites with the value depending on the volume percent of tungsten wire in the copper. For comparison, on the left is shown the strength-resistivity ratio for available electrical conductors, silver, aluminum, and copper. On the right are shown typical values for transmission cables, which are composite structures rather than composite materials. The W-Cu composites show a clear advantage. It should be pointed out, however, that on a cost basis this composite is not competitive with the standard conductors. Other combinations utilizing cheaper fibers with better conductivity than tungsten may prove to be of practical use. These W-Cu fiber composites, however, do have strength at temperatures where other

conductors are useless, and W-Cu might therefore have a use in some special applications at high temperatures.

Figure 8-35 shows the strength of some fiber composites that have been produced. Shown at the top of the figure are two conventional steel alloys for comparison, a structural steel and a high-strength alloy steel. Two classes of fiber composites are shown, fiber-reinforced metals and fiber-reinforced plastics. The volume percent of fiber in the composite is shown. Generally, if more fiber could be added, even better strengths would be achieved.

Composite data are shown for 25 percent steel wire in aluminum, 50 percent boron in aluminum, and the model system of tungsten in copper with 75 volume percent tungsten.

For plastics, NASA data (ref. 33) for filament-wound specimens of "S" glass and graphite and boron in epoxy plastic are tabulated, as well as data from other sources for glass fabric material. The strongest material is "S" glass in epoxy. All of these materials other than "E" glass are superior to structural steel in strength, but only "S" glass - epoxy has a large advantage over alloy steel. If more fiber could be added, however, all of the composite materials would show a significant advantage.

As mentioned earlier in this section, greater advantages are shown for fiber-reinforced materials if the comparisons are made on the basis of both strength and density. In figure 8-36 the same materials are shown, but because high strength and low weight are often required in aerospace applications, the comparisons are based on the strength-to-density ratio.

On the basis of that ratio many of the composites are far superior to the steels. The "S" glass epoxy has 13 times the strength-to-density ratio of structural steel and is five times better than the alloy steel. Even glass fabric material is superior to structural steel. The reason for aerospace interest in these materials is obvious. Often the strength-to-density advantage of fiberglass-reinforced plastics is of importance to nonaerospace applications. An example is the boom of the "cherry pickers" used by industry to lift and support men for work on power lines and transformers. If still another comparison were made on the basis of stiffness, the boron and graphite materials would be far superior to all other materials.

A final but important factor to consider in these materials is cost (table 8-I). Here the comparison has been made on the basis of the cost to do the job required of these materials - that is, to carry a load. Imagine that a 1-foot-long piece of material is required to carry a load of 100 000 pounds. If the material is strong, a small-diameter bar would do the job, but if it is weak, more material is required. The dollar values are the comparative numbers.

For the conventional materials the steel alloy is cheapest, costing only

28 cents for the material required. If the new high-strength maraging steels are used, the cost jumps to $1.92. An aluminum alloy is 96 cents, and titanium is $4.32. Other factors than strength alone, of course, dictate the use of higher cost materials. Aluminum is used in homes and cars, though steel would be cheaper. For aerospace applications, maraging steels, aluminum, and titanium are used because they save weight in space, and a pound saved in a vehicle headed for outer space can easily be worth $1000. Thus, initial material costs can be insignificant.

The cost shown for each fiber is that of the fiber alone, not of a fabricated composite. The cost of the glass fibers is competitive with the cheaper steels. When bar steel is converted into wire, the cost to carry a load goes up by a factor of 50, and graphite and boron are very expensive indeed. However, these latter fibers are newly developed materials, and their costs have already come down by factors of over 20 in the past 3 or 4 years. Both, but especially graphite, should decrease significantly as the market increases and production methods improve. Until then their use will be limited to aerospace.

There has already been great commercial interest in the application of glass fibers for reinforcing plastic, as would be expected from their low cost. Figure 8-37 shows a 10 000-gallon underground storage tank for gasoline. These tanks have become common at neighborhood filling stations. In addition to providing the necessary strength and light weight, glass-reinforced plastics are much cheaper than steel because of greatly superior corrosion resistance.

Figures 8-38 shows an auto trailer and a railroad tank car that have been fabricated by using the filament winding technique - exactly the technology developed for fabrication of rocket tanks. Use of fiberglass-reinforced plastic saves 9 tons of weight in a railroad car, which should mean cheaper transportation.

CONCLUDING REMARKS

In conclusion, five areas of emerging technology in engineering mechanics and materials have been summarized - areas that may be of interest to the power industry. Perhaps this presentation will stimulate more detailed discussions whereby NASA research efforts can be of further assistance on special problems of the power industry.

REFERENCES

1. Manson, S. S.; and Haferd, A. M.: A Linear Time-Temperature Relation for Extrapolation of Creep and Stress-Rupture Data. NACA TN 2890, 1953.

2. Manson, S. S.: Design Considerations for Long Life at Elevated Temperatures. Joint International Conference on Creep. Vol. II - Discussion. Institution of Mechanical Engrs., London, 1965, p. D-36.

3. Manson, S. S.: Succop, G.; and Brown, W. R., Jr.: The Application of Time Temperature Parameters to Accelerated Creep-Rupture Testing. Trans. ASM, vol. 51, 1959, pp. 911-934.

4. Mendelson, Alexander; Roberts, Ernest, Jr.; and Manson, S. S.: Optimization of Time-Temperature Parameters for Creep and Stress Rupture, with Application to Data from German Cooperative Long-Time Creep Program. NASA TN D-2975, 1965.

5. Woodyatt, L. R.; Sims, C. T.; and Beattie, H. J., Jr.: Prediction of Sigma-Type Phase Occurrence from Compositions in Austenitic Superalloys. Trans. AIME, vol. 236, no. 4, Apr. 1966, pp. 519-527.

6. Sandrock, Gary D.; Ashbrook, Richard L.; and Freche, John C.: Effect of Variations in Silicon and Iron Content on Embrittlement of a Cobalt-Base Alloy (L-605). NASA TN D-2989, 1965.

7. Sandrock, Gary D.; and Leonard, L.: Cold Reduction as a Means of Reducing Embrittlement of a Cobalt-Base Alloy (L-605). NASA TN D-3528, 1966.

8. Wolf, James S.; and Sandrock, Gary D.: Some Observations Concerning the Oxidation of the Cobalt-Base Superalloy L-605 (HS-25). NASA TN D-4715, 1968.

9. Coffin, L. F., Jr.: A Study of the Effects of Cyclic Thermal Stresses on a Ductile Metal. Trans. ASME, vol. 76, no. 6, Aug. 1954, pp. 931-950.

10. Manson, S. S.: Thermal Stress and Low-Cycle Fatigue. McGraw-Hill Book Co., Inc., 1966, p. 132.

11. Manson, S. S.: Fatigue: A Complex Subject - Some Simple Approximations. Exp. Mech., vol. 5, no. 7, July 1965, pp. 193-226.

12. Manson, S. S.; and Halford, G. R.: A Method of Estimating High-Temperature, Low-Cycle Fatigue Behavior of Metals. Presented at the International Conference on Thermal and High-Strain Fatigue, Institute of Metals, London, 1967.

13. Halford, G. R.; and Manson, S. S.: Application of a Method of Estimating High-Temperature, Low-Cycle Fatigue Behavior of Materials. Presented at the ASM National Metal Congress, Cleveland, Ohio, Oct. 19, 1967.

14. Shannon, John L., Jr.: Fracture Mechanics - Part 1. Machine Des., vol. 39, no. 23, Sept. 28, 1967, pp. 122-127.

15. Shannon, John L., Jr.: Fracture Mechanics - Part 2. Machine Des., vol. 39, no. 24, Oct. 12, 1967, pp. 188-194.

16. Anon.: Proposed Recommended Practice for Plane-Strain Fracture Toughness Testing of High-Strength Metallic Materials Using a Fatigue-Cracked Bend Specimen. ASTM Standards, Part 31, 1968, pp. 1018-1030.

17. Anon.: Fracture Toughness Testing and Its Applications. Spec. Tech. Publ. No. 381, ASTM, 1965, pp. 1-2, 133-196.

18. Fisher, Douglas M.; Bubsey, Raymond T.; and Srawley, John E.: Design and Use of Displacement Gage for Crack-Extension Measurements. NASA TN D-3724, 1966.

19. Brown, W. F., Jr.; and Srawley, J. E.: Plane Strain Crack Toughness Testing of High Strength Metallic Materials. Spec. Tech. Publ. No. 410, ASTM, 1967.

20. Srawley, J. E.; Jones, M. H.; and Brown, W. F., Jr.: Determination of Plane Strain Fracture Toughness. Mat. Res. & Standards, vol. 7, no. 6, June 1967, p. 262.

21. Pierce, William S.: Crack Growth in 2014-T6 Aluminum Tensile and Tank Specimens Cyclically Loaded at Cryogenic Temperatures. NASA TN D-4541, 1968.

22. Sullivan, Timothy L.: Uniaxial and Biaxial Fracture Toughness of Extra-Low Interstitial 5Al-2.5Sn Titanium Alloy Sheet at 20° K. NASA TN D-4016, 1967.

23. Sullivan, Timothy L.; and Orange, Thomas W.: Continuity Gage Measurement of Crack Growth on Flat and Curved Surfaces at Cryogenic Temperatures. NASA TN D-3747, 1966.

24. Orange, Thomas W.: Evaluation of Special 301-Type Stainless Steel for Improved Low Temperature Notch Toughness of Cryoformed Pressure Vessels. NASA TN D-3445, 1966.

25. Ault, G. Mervin; and Burte, H. M.: Technical Applications for Oxide-Dispersion Strengthened Materials. Presented at the AIME Conference on Oxide Dispersion Strengthening, Bolton Landing, N. Y., June 27, 1966.

26. Weeton, John W.; and Quatinetz, Max: Cleaning and Stabilization of Dispersion Strengthened Materials. Presented at the AIME Conference on Oxide Dispersion Strengthening, Bolton Landing, N. Y., June 27, 1966.

27. Anon.: TD Nickel Dispersion Strengthened Nickel. Rep. A-27045, Dupont Metal Products, New Product Information.

28. McDonald, Allen S.: A Dispersion Hardened Copper for Electrical Uses. Metal Progress, vol. 89, no. 4, Apr. 1966, pp. 70-72.

29. Ashbrook, Richard L.; Hoffman, Anthony C.; Sandrock, Gary D.; and Dreshfield, Robert L.: Development of a Cobalt-Tungsten Ferromagnetic, High-Temperature, Structural Alloy. NASA TN D-4338, 1968.

30. Weeton, John W.; and Signorelli, Robert A.: Fiber-Metal Composite Materials. NASA TN D-3530, 1966.

31. Petrasek, Donald W.; Signorelli, Robert A.; and Weeton, John W.: Refractory Metal Fiber Nickel Alloy Composites for Use at High Temperatures. Presented at the Society of Aerospace Material and Process Engineers 12th National Symposium, Orange County, Calif., Oct. 10-12, 1967.

32. McDanels, David L.: Electrical Resistivity and Conductivity of Tungsten-Fiber-Reinforced Copper Composites. NASA TN D-3590, 1966.

33. Hanson, Morgan P.: Glass-, Boron-, and Graphite-Filament-Wound Resin Composites and Liners for Cryogenic Pressure Vessels. NASA TN D-4412, 1968.

TABLE 8-I. - COST OF FIBERS COMPARED

TO CONVENTIONAL MATERIALS

Materials	Cost of 1-ft-long bar to carry 100 000-lb load
Conventional:	
Steel (structural)	$ 0.28
(304 SS)	1.81
(maraging)	1.92
Aluminum (6061)	.96
Titanium (6Al-4V)	4.32
Fibers:	
"E" glass	0.12
"S" glass	.17
SiO_2 (quartz)	3.40
Steel (rocket wire)	8.40
Graphite (RAE)	62.00
Boron	115.00

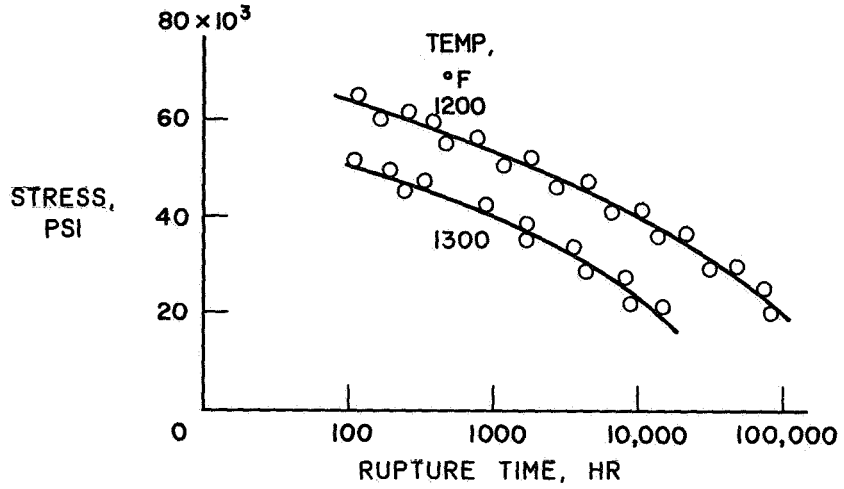

Figure 8-1. - Stress to rupture.

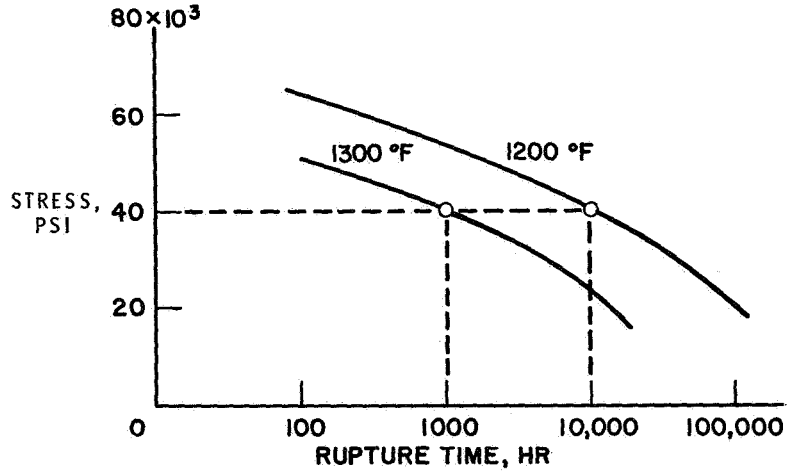

Figure 8-2. - Reduction of test time by increasing temperature.

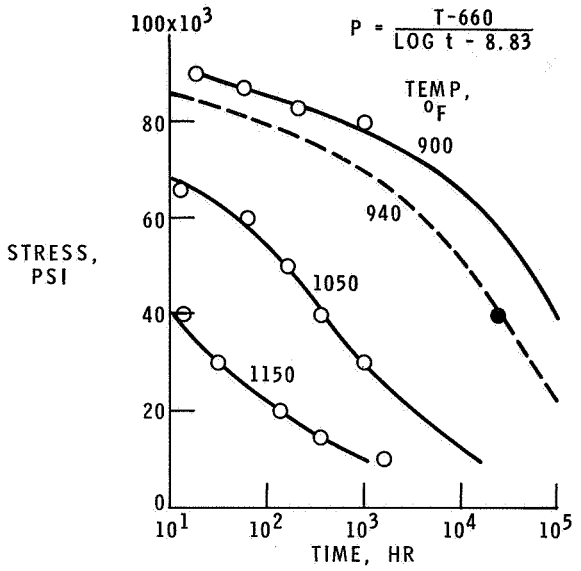

Figure 8-3. - Use of Manson-Haferd parameter to interpolate and extrapolate data.

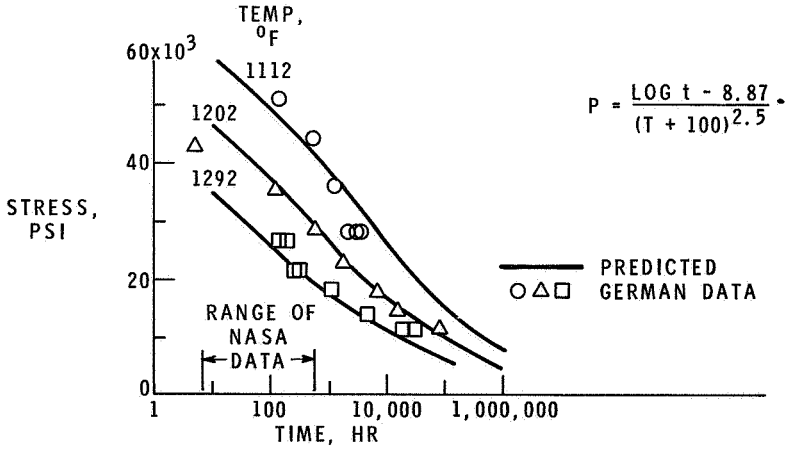

Figure 8-4. - Parameter extrapolations for German steel based on short-time NASA data.

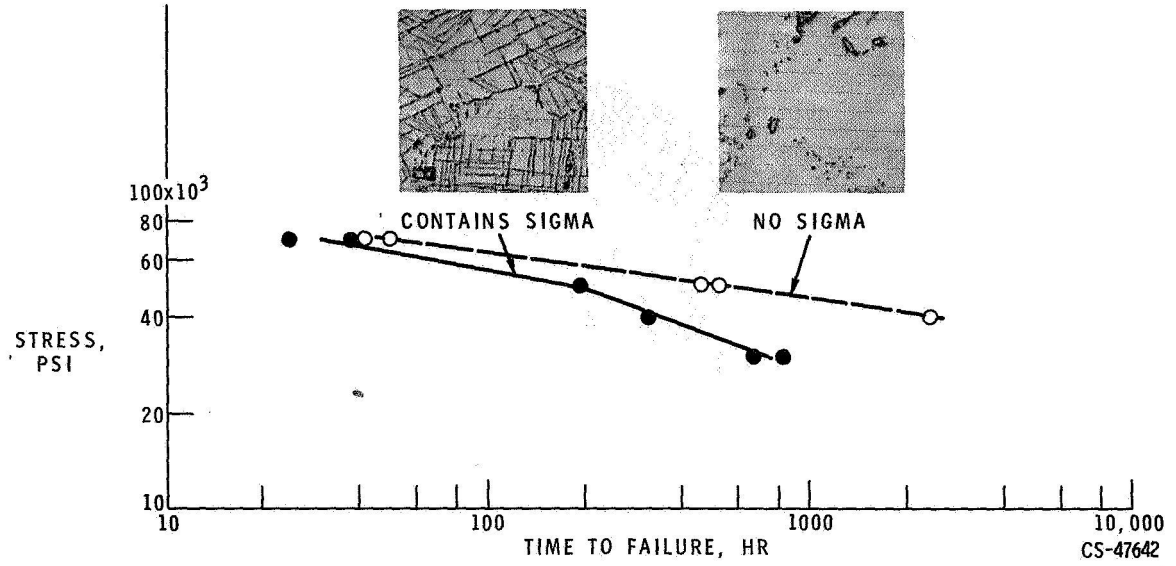

Figure 8-5. - Influence of metallurgical instability on long-time strength (1550° F).

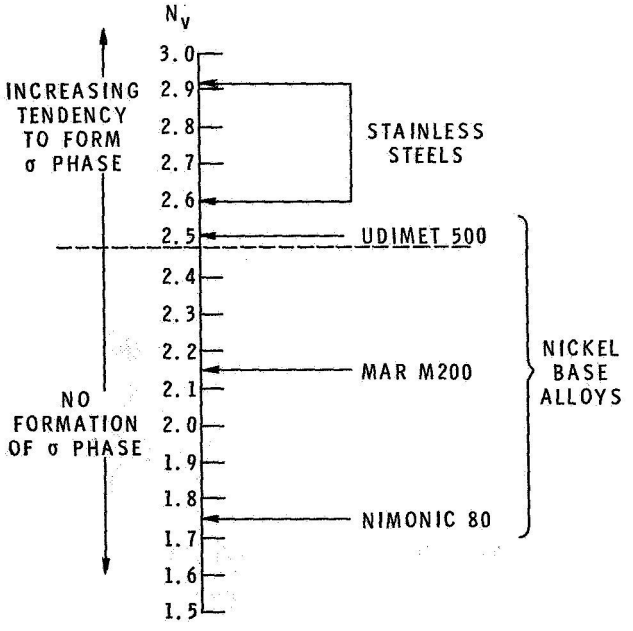

Figure 8-6. - Prediction of sigma formation from N_v calculation where N_v is function of elements in alloy and their electron vacancy.

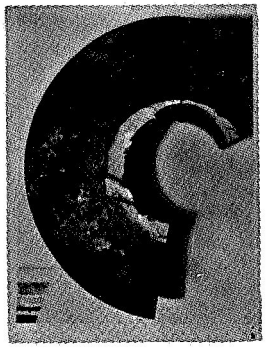

CS-47639

Figure 8-7. - Thermal fatigue failure of superheater nozzle connection.

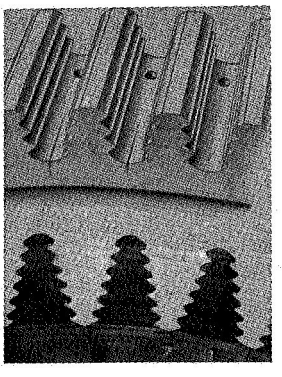

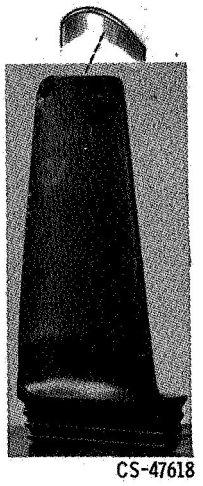

CS-47618

TURBINE DISK TURBINE BUCKET

Figure 8-8. - Typical thermal fatigue failures.

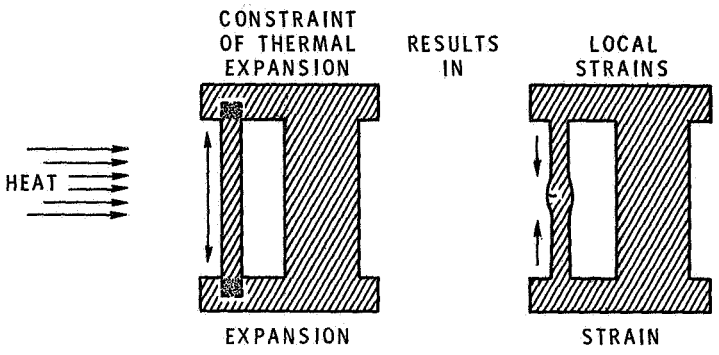

Figure 8-9. - Mechanism of thermal fatigue.

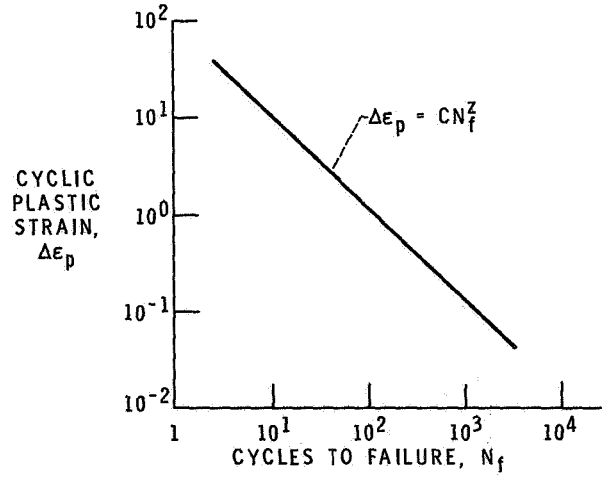

Figure 8-10. - Manson-Coffin rule for plastic fatigue.

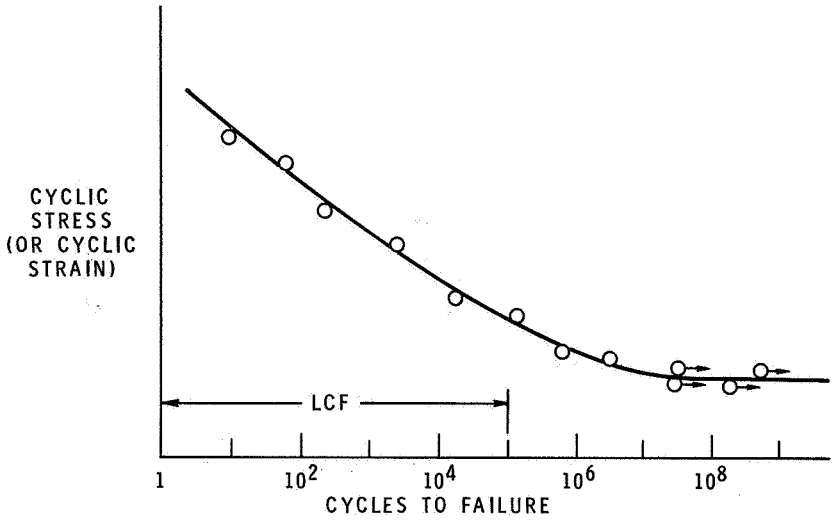

Figure 8-11. - Typical fatigue curve.

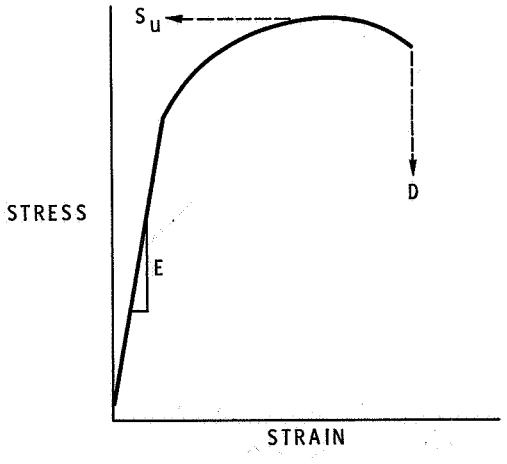

Figure 8-12. - Short-time tensile curve.

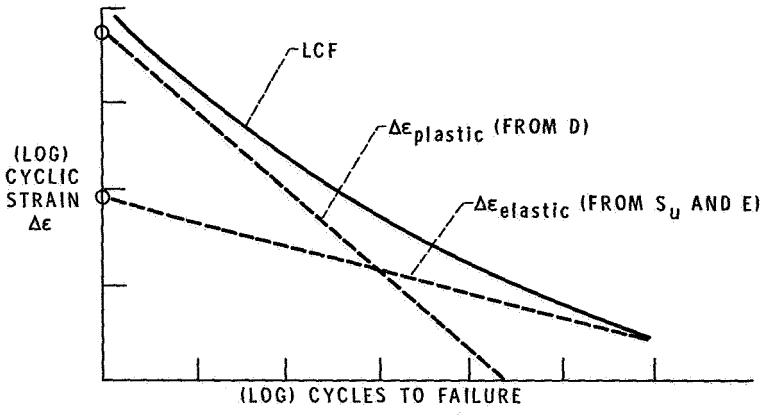

Figure 8-13. - Prediction of low-cycle fatigue from tensile test by method of universal slopes.

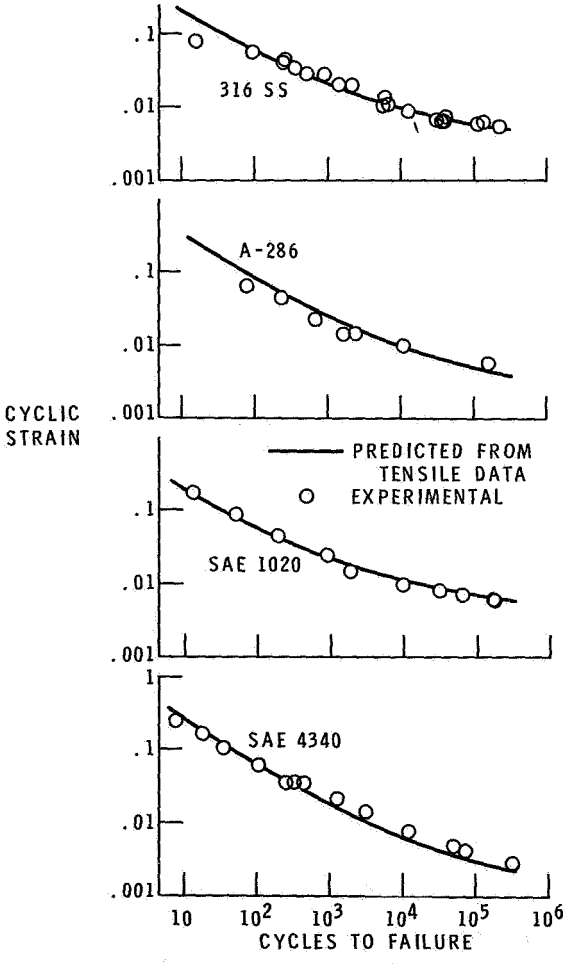

Figure 8-14. - Prediction of low-cycle fatigue from short-time tensile test.

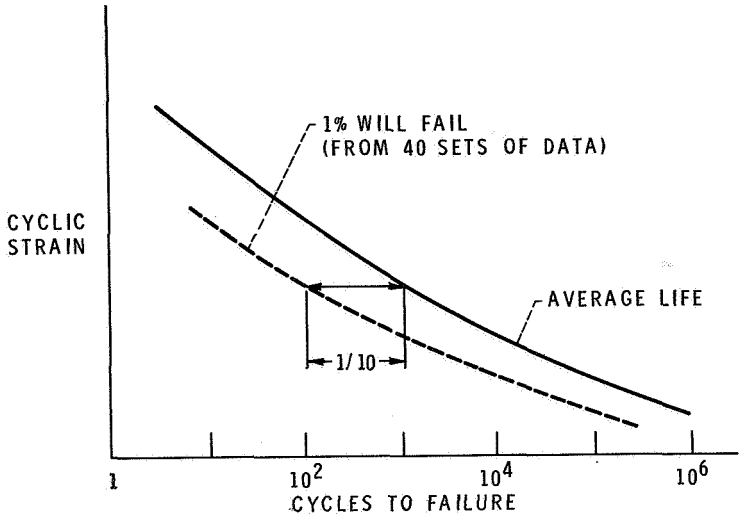

Figure 8-15. - Estimation of low-cycle fatigue at high temperature by universal slopes 10 percent rule.

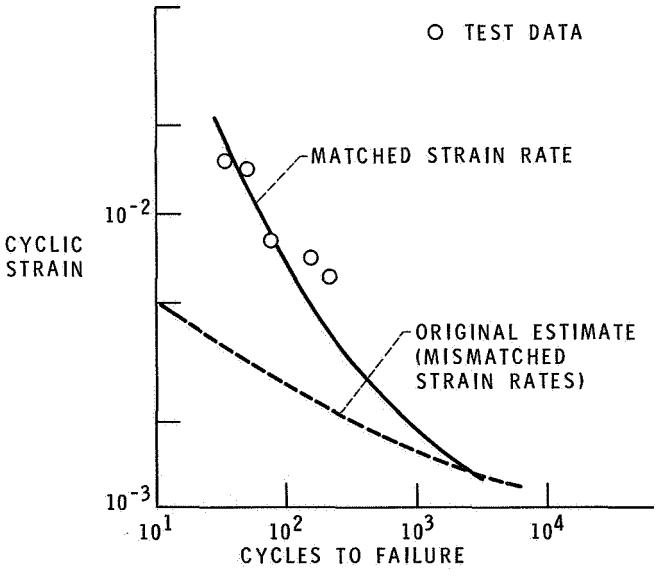

Figure 8-16. - Improved estimate of high-temperature low-cycle fatigue.

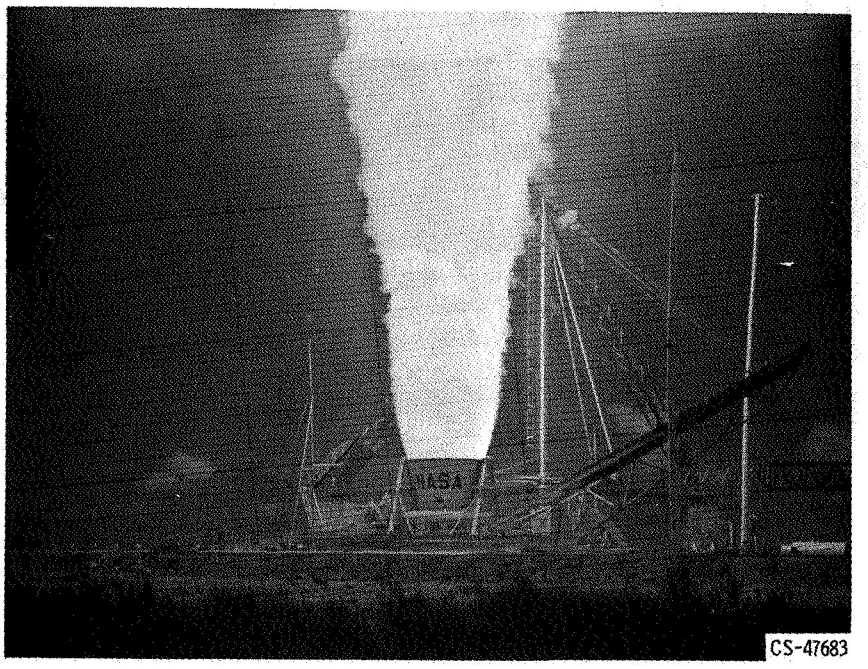

Figure 8-17. - Solid-propellant 260-inch-diameter rocket.

Figure 8-18. - Case for 260-inch solid rocket motor.

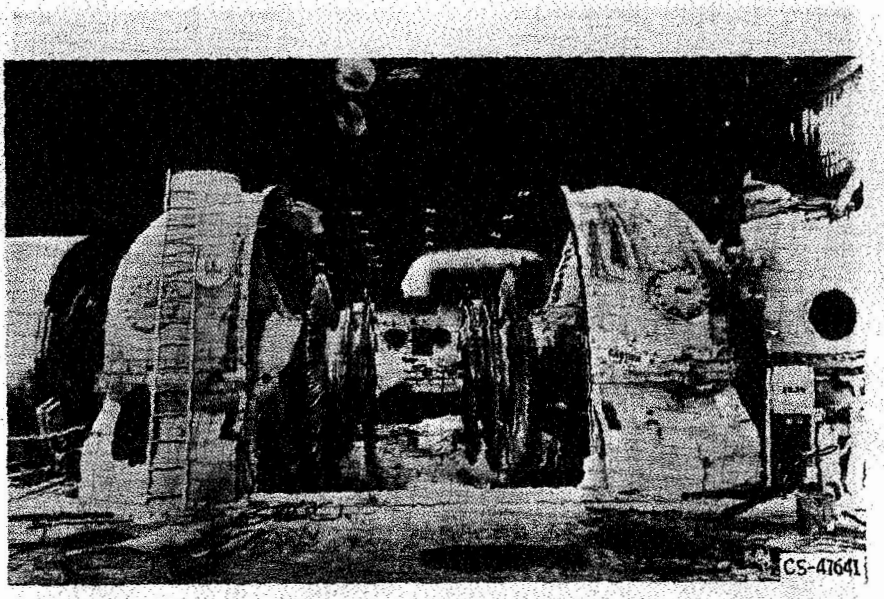

Figure 8-19. - Failure of steam turbine.

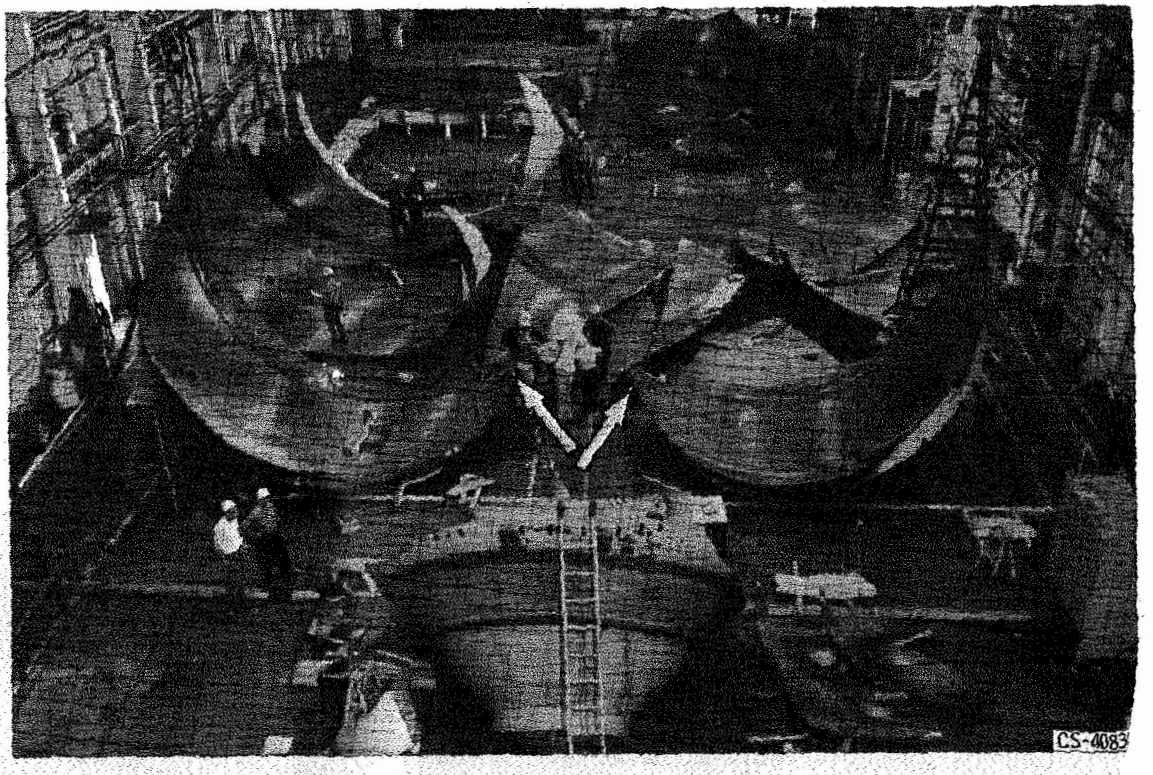

Figure 8-20. - Failed 260-inch rocket motor case.

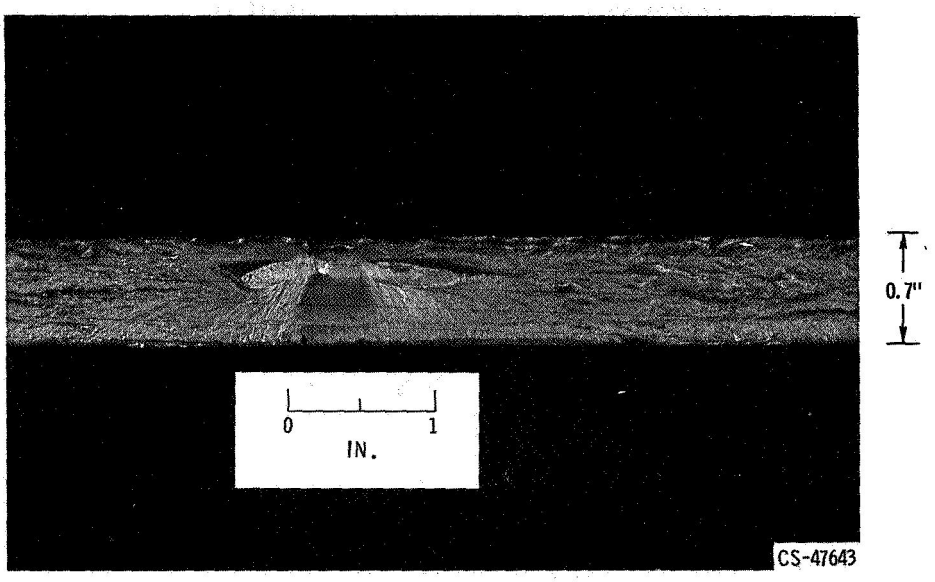

Figure 8-21. - Flaw at which fracture initiated.

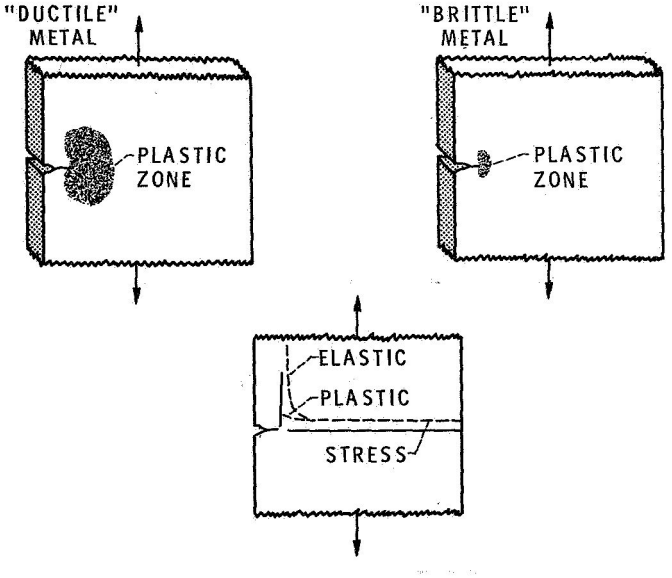

Figure 8-22. - Brittle fracture of metals.

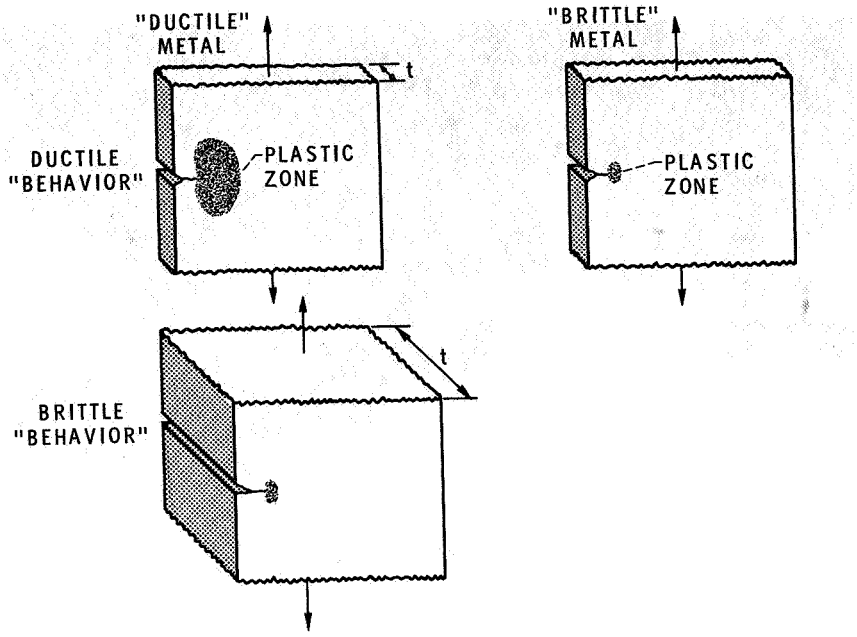

Figure 8-23. - Variation of fracture with part geometry.

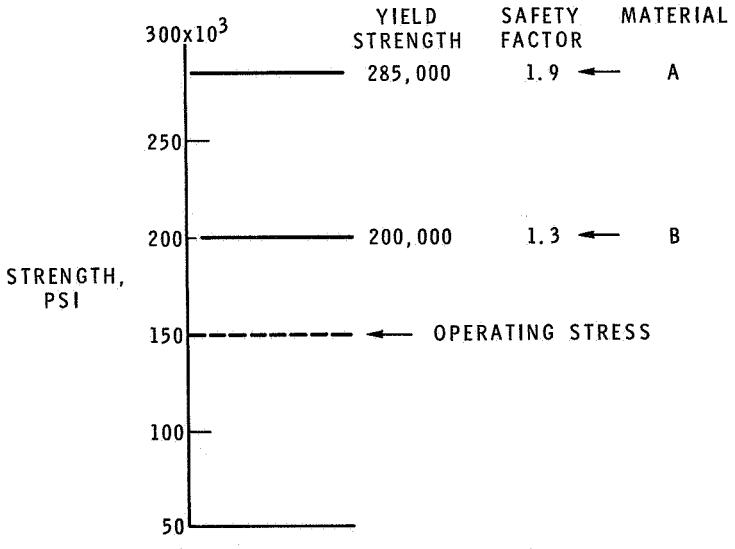

Figure 8-24. - Conventional comparison of materials based on safety factor.

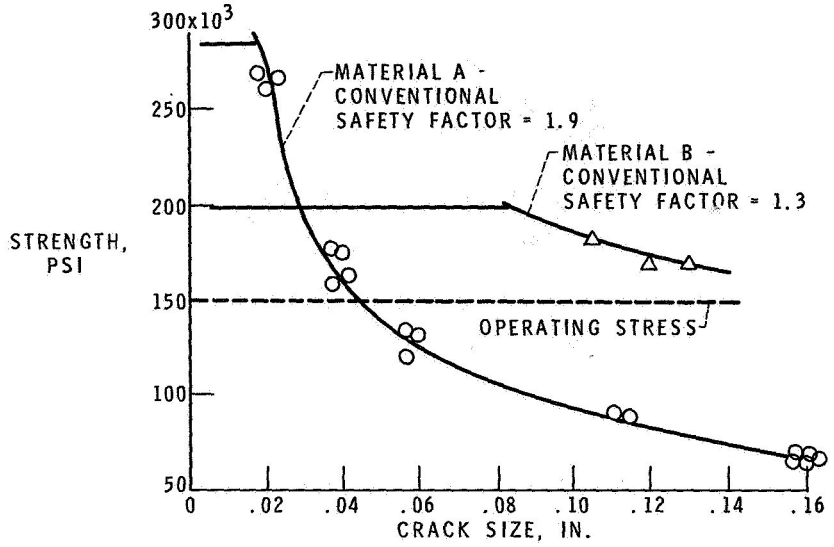

Figure 8-25. - Importance of considering material flaws or cracks in design.

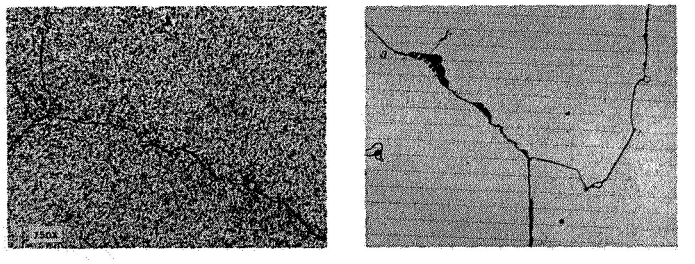

Figure 8-26. - Microstructure of typical high-temperature alloy.

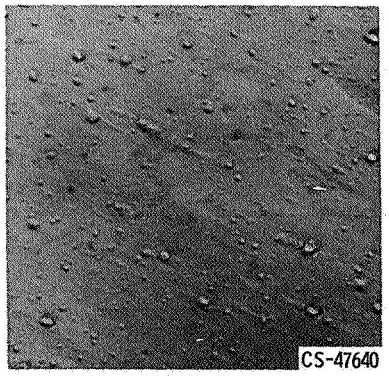

Figure 8-27. - Dispersion-strengthened superalloy ($Ni + ThO_2$).

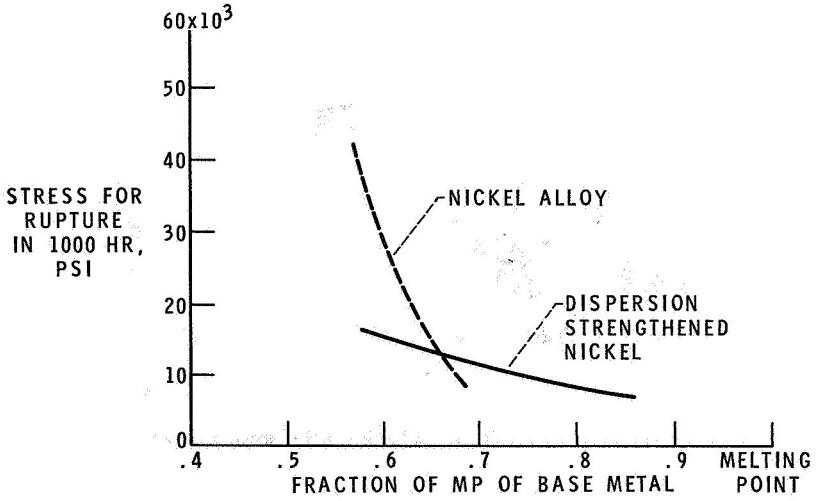

Figure 8-28. - Dispersion-strengthened metals retain strength to higher temperatures.

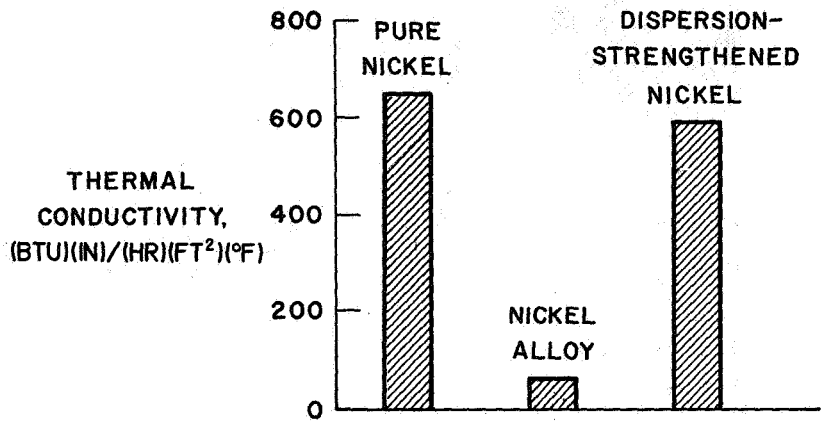

Figure 8-29. - Dispersion-strengthened pure metals maintain excellent conductivity.

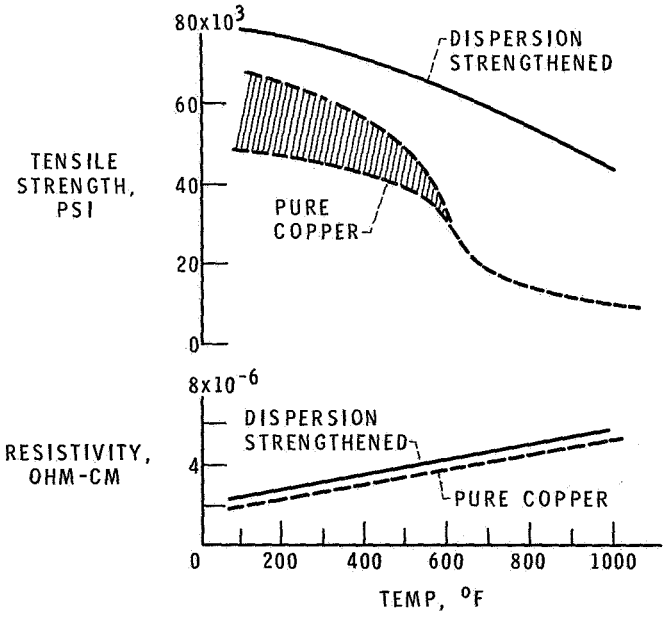

Figure 8-30. - High-temperature strength and low resistivity with dispersion strengthening.

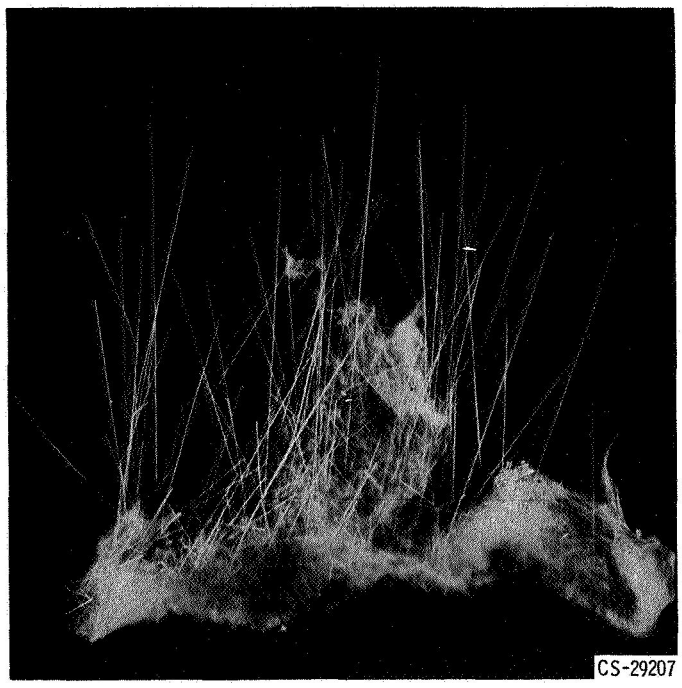

Figure 8-31. - Sapphire (Al_2O_3) whiskers.

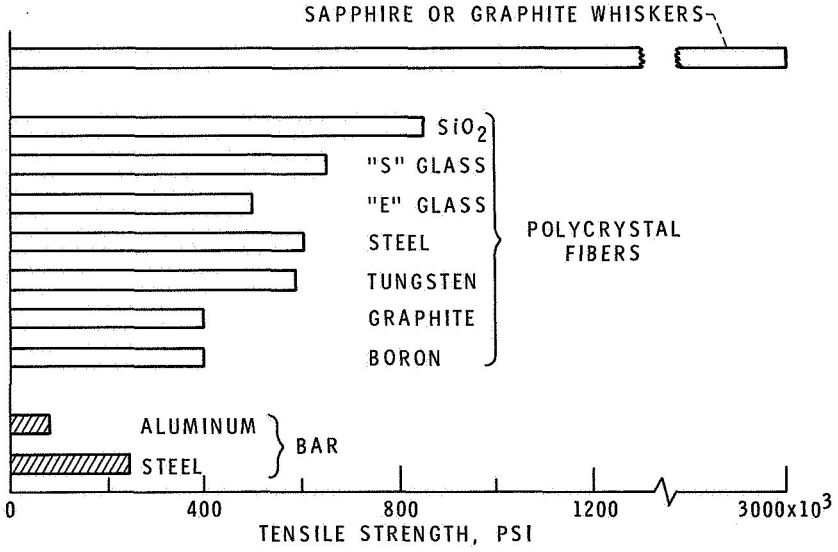

Figure 8-32. - Strength of fibers.

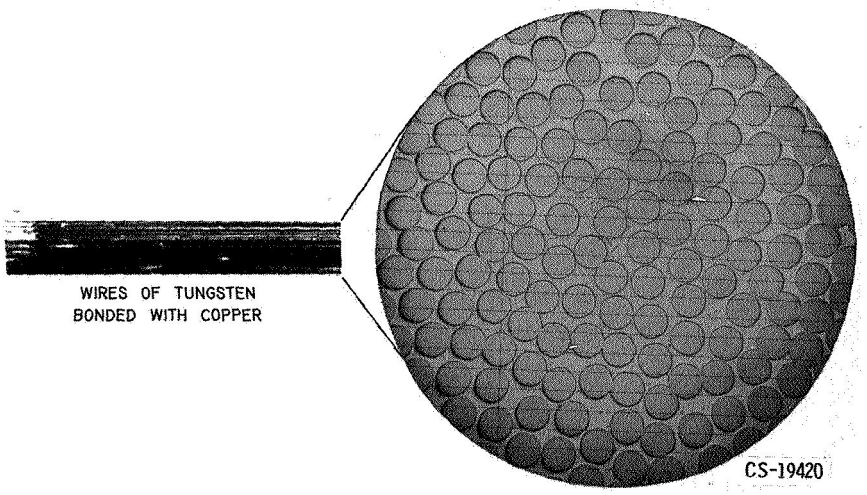

Figure 8-33. - Composite materials from metal fibers.

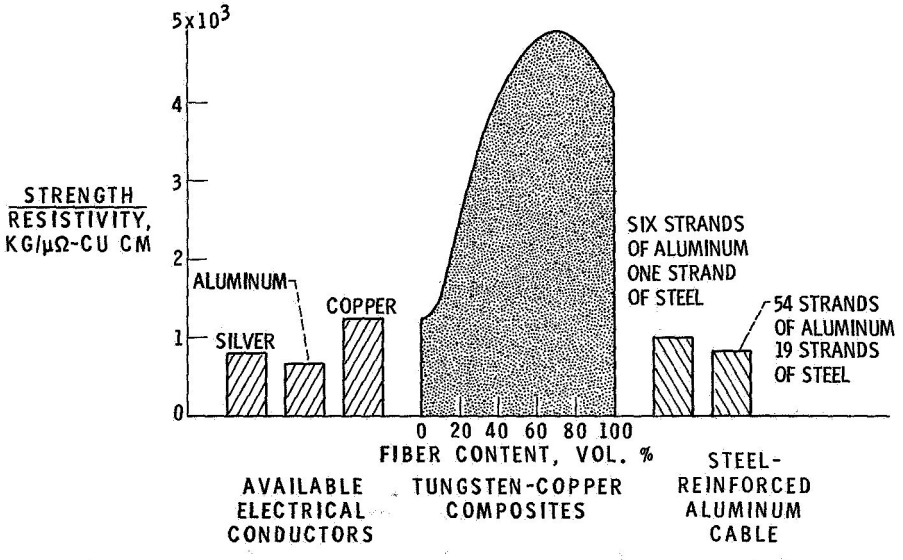

Figure 8-34. - Comparison of tungsten-fiber-reinforced copper composites with other electrical conductors.

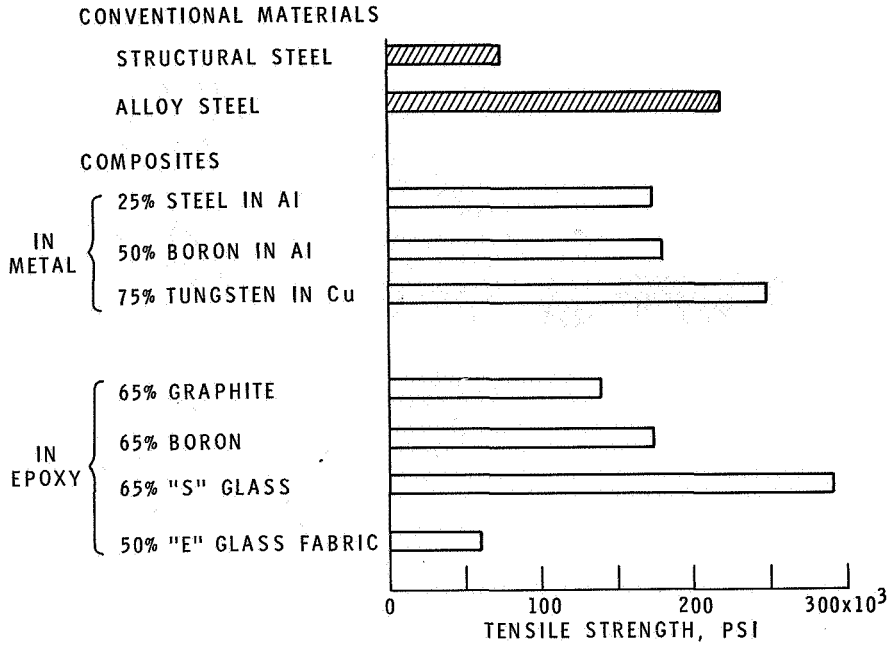

Figure 8-35. - Tensile strength of composites.

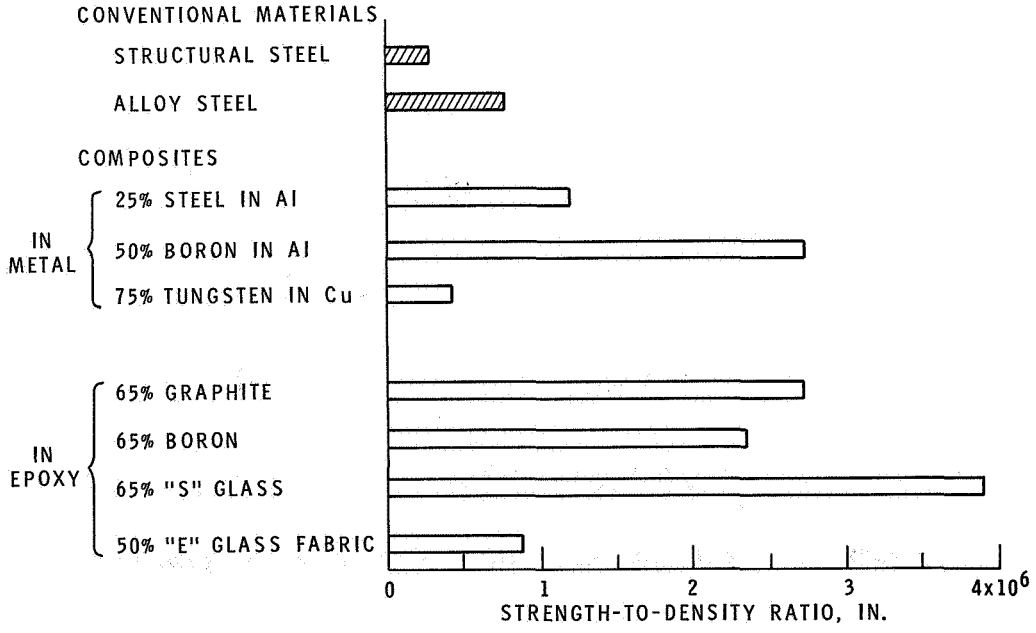

Figure 8-36. - High strength-to-density ratios of composites.

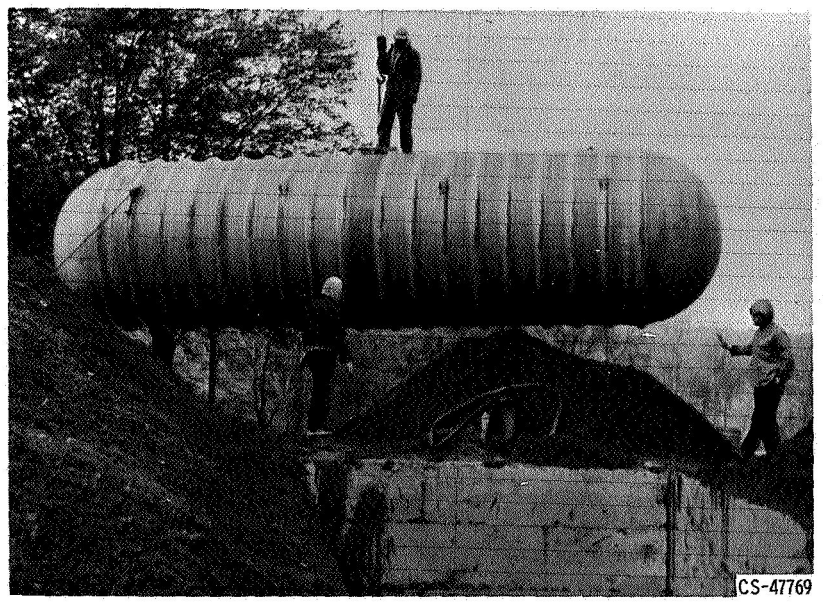

Figure 8-37. - Fiberglass-reinforced 10,000-gallon plastic tank for underground storage.

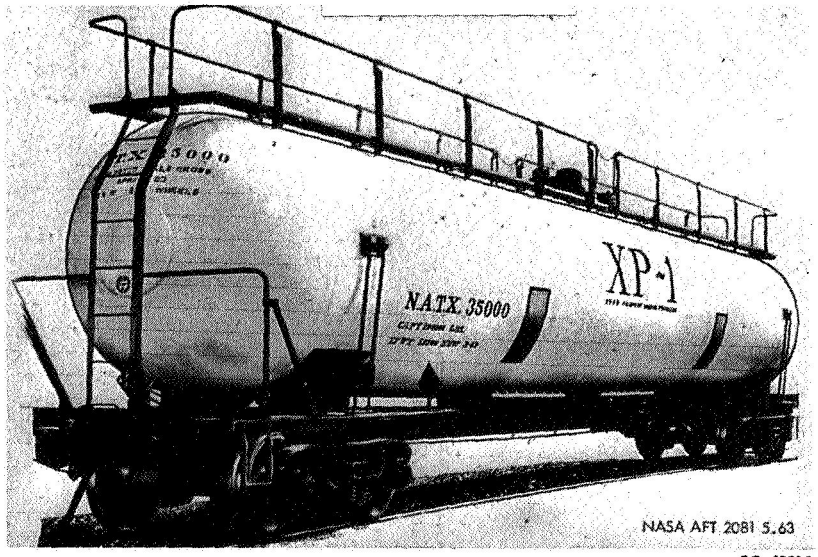

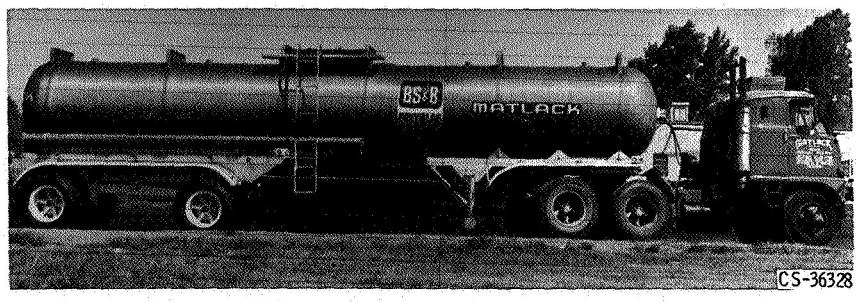

Figure 8-38. - Filament-wound glass-reinforced plastic tanks.